Chapter 4

Gap Structures of A-15 Alloys from the Superconducting and Normal-State Break-Junction Tunnelling

Toshikazu Ekino, Alexander M. Gabovich,
Akira Sugimoto, Yuta Sakai and Jun Akimitsu

Additional information is available at the end of the chapter

http://dx.doi.org/10.5772/59338

Introduction

A well-known A-15 compound Nb_3Sn was investigated by the break-junction tunnelling technique with high superconducting critical temperature $T_c \approx 18$ K. Relevant energy-gap values were measured at $T = 4.2$ K and these manifested as conductance peaks at bias voltages $2\Delta/e = 4$–6 mV. Here, T is temperature and $e > 0$ is the elementary charge. In addition to superconductivity-driven gap structures, reproducible humps were also detected at biases ±20–30 mV and ±50–60 mV for $T = 4.2$ K. Such hump features, complementary to coherent peaks at the superconducting-gap edges, apparently resemble the pseudo-gap manifestations inherent to high-T_c superconductors. These humps remain the only gap-related features above T_c. Possible origins of these structures are discussed with emphasis on the charge–density–wave (CDW) formation. CDWs are accompanied by periodic lattice distortions and are related to the structural phase transition discovered decades ago in Nb_3Sn. The current-voltage characteristics exhibit asymmetries, being probably a consequence of normal-metal junction shores or due to the vanishing symmetry of the junction conductance when CDWs are present in both electrodes.

PACS numbers: 74.55.+v, 74.70.Ad, 71.20.-b, 74.81.Fa, 81.30.Kf

Materials with A-15 (β-tungsten) crystal structure [1, 2] possessed the highest superconducting critical temperatures, T_c, over a long period of time until Cu-based superconducting ceramic oxides were discovered [3]. The compound Nb_3Sn is a representative material with $T_c \approx 18$ K among those inter-metallic alloy compounds and possesses stable metallurgical characteristics [1, 2]. Therefore, Nb_3Sn and some other older and newer materials, such as MgB_2 and Fe-based superconductors, are competitive with cuprates in technological applications of superconductivity [4–11].

The crystal structure of Nb_3Sn (as well as of its A-15 relatives) is not a layered one as that of the copper-oxide or Fe-based high T_c superconductors. Instead, it includes orthogonal linear chains of Nb atoms along each principal cube axis direction [1, 2] (see Figure1). This quasi-one-dimensional feature served as a guide for the Labbe–Friedel model, which predicted structural anomalies driven by peculiarities of the normal-state electron density of states, $N(E)$, near the Fermi level (a cooperative Jahn–Teller effect). More involved Gor'kov model, taking into account *inter alia* the inter-chain correlations, also leads to the $N(E)$ singularity and a Peierls phase transition. Whatever the theoretical details, the primordial (high-temperature, high-T) electron spectrum in Nb_3Sn is unstable towards low-T phase transformation [12].

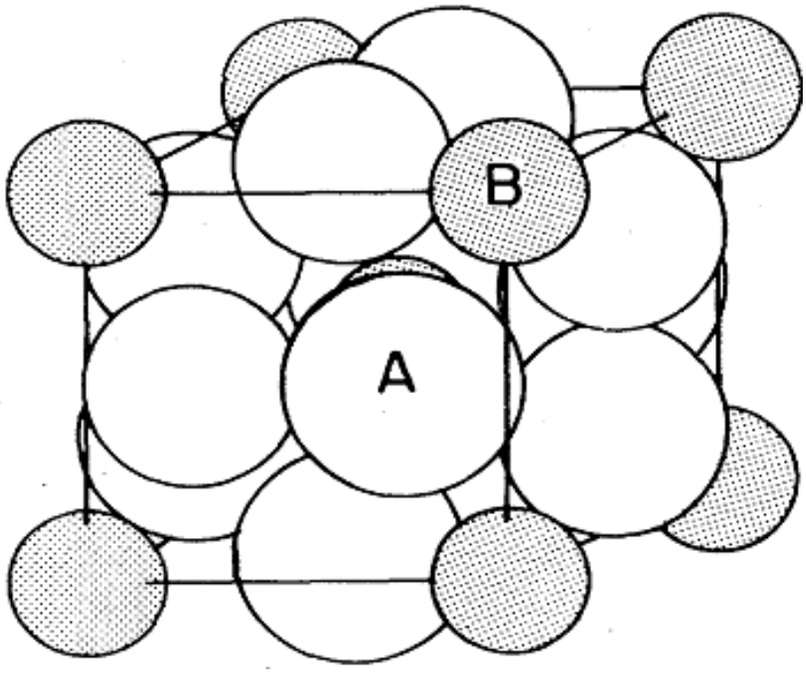

Figure 1. The A-15 crystal structure for the compound formula A_3B. In our case, A stands for Nb whereas B stands for Sn (taken from Ref. [1]).

In fact, A-15 cubic compounds, including Nb_3Sn, are well known to undergo tetragonal distortion below a certain temperature T_m, being higher than T_c. Hence, some part of the Fermi surface is gapped by CDWs, which is detrimental to superconductivity, because of the reduced electron density of states, which to a large extent determines T_c. The interplay between periodic lattice distortions accompanied by CDWs in the electron subsystem, on the one hand, and superconductivity, on the other hand, was intensively studied both experimentally and theoretically and applied to Nb_3Sn as a particular case [1, 2, 12–15].

The contest between superconducting and CDW (dielectric) order parameters should inevitably lead to a superposition of the corresponding energy gaps in the overall electron spectrum modified by both Cooper and electron–hole pairings. Any experimental technique measuring the gapped electron density of states below T_c or the convolution with its counterpart (if any) should be sensitive to the interplay between phenomena discussed above [15–17]. A typical

http://dx.doi.org/10.5772/59338

example of such a method is electronic quasi-particle tunnelling spectroscopy. Moreover, if multiple gaps of the same nature (usually, those are recognized as superconducting gaps) are inherent to the reconstructed electron spectrum or multiple gaps are generated by some kind of proximity effect, they would influence the tunnel conductance together [18–20]. Multiple superconducting gapping in Nb_3Sn was also suggested on the basis of heat capacity [21, 22] and point-contact conductivity [23] measurements. On the contrary, subsequent heat capacity studies were considered as manifestations of a single superconducting gap [24].

The origin of superconductivity and the gapping features in A-15 compounds have been explored by various methods. Namely, fabrication of corresponding tunnel junctions and electron tunnelling spectroscopic measurements were intensively carried out to probe the electron–phonon interaction in terms of the Fröhlich–Eliashberg function $\alpha^2F(\omega)$ and to extract the superconducting-gap values 2Δ [25–29]. Those junctions made for tunnelling spectroscopy purposes included artificial oxide barriers that might cause spurious features in the tunnelling spectra. On the other hand, pristine junctions of Nb_3Sn samples such as break junctions or cleaner direct contacts turned out to be of better quality so that the ambiguous influence of the barrier was avoided both in the tunnel [30] and point-contact [31] conductivity regimes. Those measurements revealed a single clear-cut superconducting gap and another feature at higher voltages most probably connected with the structural transition discussed above. In this chapter, tunnelling measurements of Nb_3Sn single crystals are presented using a break-junction technique that has been improved on the basis of previous work [30]. The experiments were carried out focusing on both the superconducting-gap characteristics and the electronic peculiarities of $N(E)$ emerging due to the structural (martensitic) transition intimately associated with CDWs. The latter could be due to the Peierls [1–3, 12] or excitonic (Coulomb) [32] transitions of the parent high-T state. In the mean-field approach, the coupled system of equations describing competing superconducting and electron–hole pairings is the same for any microscopic picture of the CDW pairing [13–15, 33]. Therefore, the consequences important for our subsequent analysis are similar for both kinds of electron–hole instabilities at this semi-phenomenological level, although one should bear in mind the necessity of the microscopic justification for any adopted model (see, e.g., electron band calculations [34, 35]). According to earlier findings in the point-contact measurements [31], we expected the manifestations of CDWs also in the quasi-particle conductance $G(V) = dI/dV$, where I denotes the quasi-particle tunnel current across the break junction. The quantity $G(V)$ in CDW superconductors is a complicated functional of the superconducting, Δ, and dielectric (CDW), Σ, energy gaps [15, 16, 33] being no more a simple convolution of the electron density of states as in the conventional Bardeen–Cooper–Schrieffer (BCS) model of superconductivity [36]. From the experimental point of view, tunnel conductances $G(V)$ distorted by CDW gapping are well known for a number of relevant materials [15, 16, 37, 38].

2. Experimental procedures

Nb_3Sn single crystal samples were grown by a standard vapour transport method. The temperature dependence of the electrical resistance for an Nb_3Sn crystal is shown in Figure 2.

It was measured using the break-junction configuration just before the breaking. To avoid any difficulty in forming a clean junction interface on the small surface area of the tiny crystalline piece, making such a break junction is the best method. A cryogenic fracture at 4.2 K of the crystal piece provides the crucial advantage of this technique. The fracture is performed by at first mounting the sample on the flexible substrate with four electrodes, subsequently stressed by an external bending force. Thus, a fresh and clean junction interface appears that can provide the undistorted gap features both for superconducting and semiconducting electron spectra including extremely surface-sensitive delicate compounds [38]. This junction design exhibits the symmetric superconductor–insulator–superconductor (SIS) geometry.

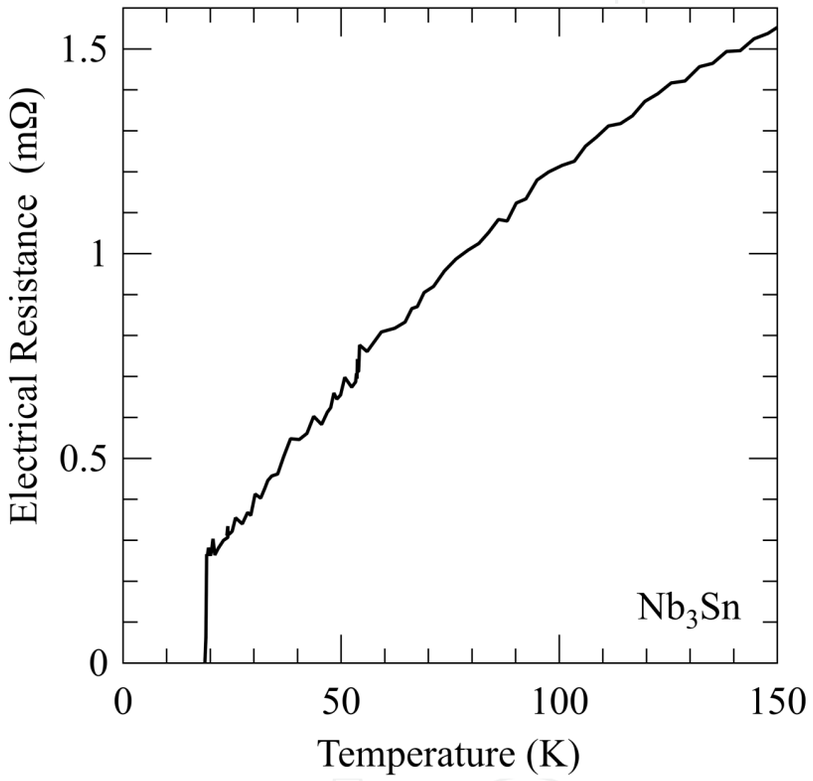

Figure 2. The temperature dependence of the electrical resistance, *R* (*T*), for Nb_3Sn used in the present break-junction measurements.

3. Results and discussion

The tunnelling conductance $G(V) = dI/dV(V)$ in the superconducting state at $T = 4.2$ K is shown in Figure 3 for several break junctions. The sharp and intensive gap-edge structure observed in Figure 3 (a) exhibits the *peak-to-peak* voltage interval $V_{p\text{-}p} \approx 8.6$ mV (corresponding to bias voltages $V_p \approx \pm 4.3$ mV) and very small zero-bias leakage. This is common to the *s*-wave BCS gap structure inherent to the SIS geometry of the break junction, for which $V_{p\text{-}p} = 4\Delta/e$. Here $e > 0$ is the elementary charge.

http://dx.doi.org/10.5772/59338

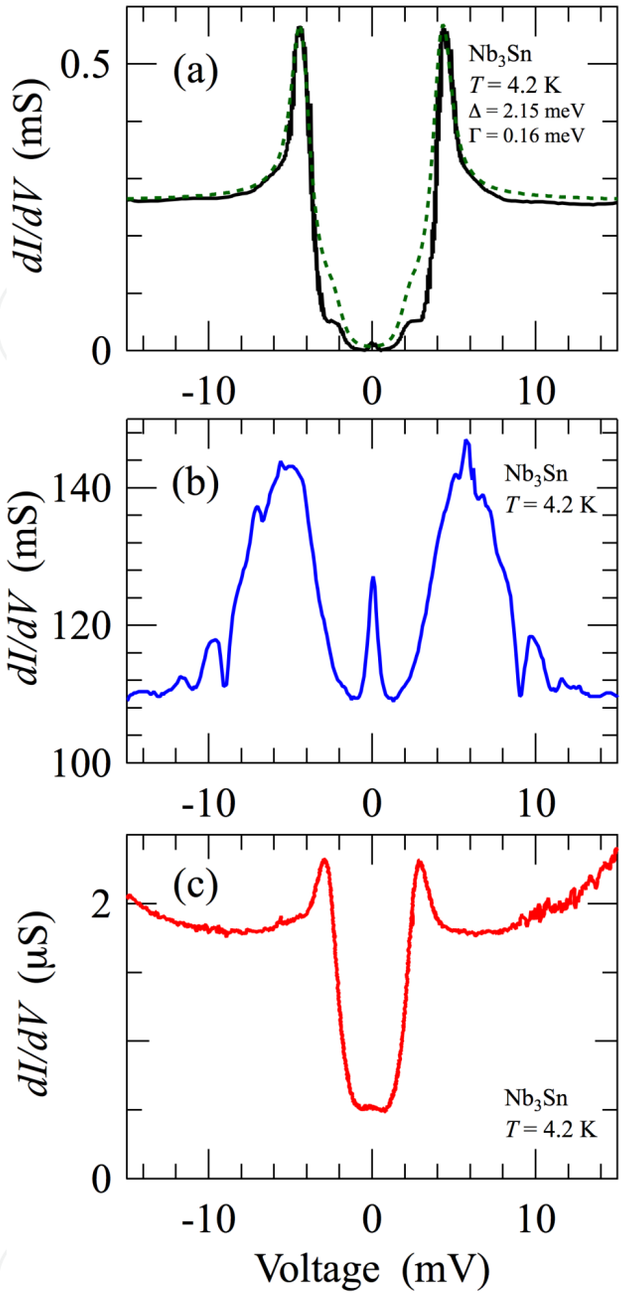

Figure 3. Conductance $G(V) = dI/dV$ obtained for different Nb_3Sn break junctions (a), (b) and (c). Tunnelling quasi-particle gap feature (a) is fitted with the broadened BCS density of states $N(E, \Gamma)$ (see the text). $G(V)$ of (b) is broadened showing much more conductance leakage as compared with (a). Substantial zero-bias leakage with asymmetric background conductance is seen in (c).

By employing the standard broadening in the quasi-particle density of states, $N(E,\Gamma) = |\mathrm{Re}\{(E-i\Gamma)/[\Delta^2-(E-i\Gamma)^2]^{1/2}\}|$, along with thermal smearing, the fitting procedure quantitatively reproduces the SIS spectral features. Here, Γ is a phenomenological broadening parameter [39]. Applying the fitting procedure, we emphasized on either the outer or the inner features of the gap structure. The resultant parameters Δ were similar in both cases, whereas Γ values describing the pair breaking caused by an identified reason varied conspicuously. The sub-

gap shoulders at ±2.3 mV in Figure 3 (a) correspond to ± Δ/e singularities as a result of the SIN admixture to $G(V)$. Here, N stands for the normal metal. In contrast to the SIS junction characteristics in Figure 3 (a), the gap peak in $G(V)$ of Figure 3 (b) is substantially broadened showing much more intensive conductance leakage as well as the high-bias conductance magnitude about 10^3 times larger than that for the junction of Figure 3 (a). The conductance leakage level reaches almost the normal-state high-bias value exhibiting also the Josephson or weak link peak at zero bias. This feature is no longer a standard tunnelling phenomenon appropriate to junctions with small transparencies [36]. Instead, the Andreev reflection at the interfaces should govern the current through the junction interface. At the same time, the wide conductance peaks at about ±5.5 mV corresponding to the values ±2Δ/e for an SIS junction do not differ much from their counterparts seen in Figure 3 (a). We rarely observed much smaller gap-peak energies. In fact, the shoulders at ±2.3 mV in Figure 3 (a) appear as the apparent but less enhanced gap-peak structures at the same bias positions in Figure 3 (c), where the substantial zero-bias leakage (~28% of the high-bias normal state) as well as the asymmetric conductance background above the gap voltages are evident. These features indicate that the tunnelling conductance of Figure 3 (c) is due to the accidental formation of an SIN junction corresponding to the peak positions of ±Δ/e, in which one side of the junction is a normal metal. Assuming the weak-coupling isotropic BCS gap to T_c ratio $2\Delta/k_BT_c \approx 3.5$, where k_B is Boltzmann constant, the observed gap values correspond to the local critical temperatures $T_c^* \approx 14.2$ K (a) and 18 K (b). The former value indicates the existence of the non-stoichiometric patch, nevertheless exhibiting almost textbook-coherent gap-edge peaks, while the latter value is close to the bulk T_c. The smaller gap value extracted from Figure 3 (a) and (c) most probably corresponds to the reported Sn-deficient phase [28], which is suggested to exist as a quite stable crystallographic phase of this compound. We note that in the present break-junction measurements, the observed maximum gap size shown in Figure 3 (b) demonstrates the almost BCS value, so that we could not find any apparent strong-coupling feature showing the typical ratios $2\Delta/k_BT_c \approx 4.3$–$4.4$ [10, 11, 28].

In Figure 4 (a), the conductance $G(V)$ is shown for two different break junctions at $T = 4.2$ K and bias voltages extended to higher regions of ±40 mV. The well-developed gap peaks, which are consistent with the results depicted in Figure 3 (a), are clearly seen. The intensive $G(V)$ peaks of the curve A are cut in order to magnify other important features. The reproducible appearance of the peaks at ±4.2–4.6 mV as is shown in Figure 4 (a) suggests that the cracking forming break junctions tends to occur along the defect phase of the crystal [28]. In curve A, outer peaks appear at values ≈ ±5.5 mV, which can be seen as shoulders in curve B. These features are consistent with the broad peaks corresponding to the bulk T_c as was discussed while describing Figure 3, thereby reflecting the inherent gap value of Nb_3Sn, although those coherent gap peaks are not very strong. The outer-bias peaks or shoulders in curves A or B appear when the zero-bias peak is present. Since zero-bias peaks are manifestations of the coherent Cooper-pair tunnelling and are not expected to appear in the distorted regions, the presence of this feature supports the idea that the break-junction interface is formed inside an optimal superconducting-phase patch of the inhomogeneous Nb-Sn composite displaying substantial gap distributions. Thus, multiple superconducting gaps are indeed observed in Nb_3Sn, being, however, a consequence of the spatial inhomogeneity and, probably, also certain

http://dx.doi.org/10.5772/59338

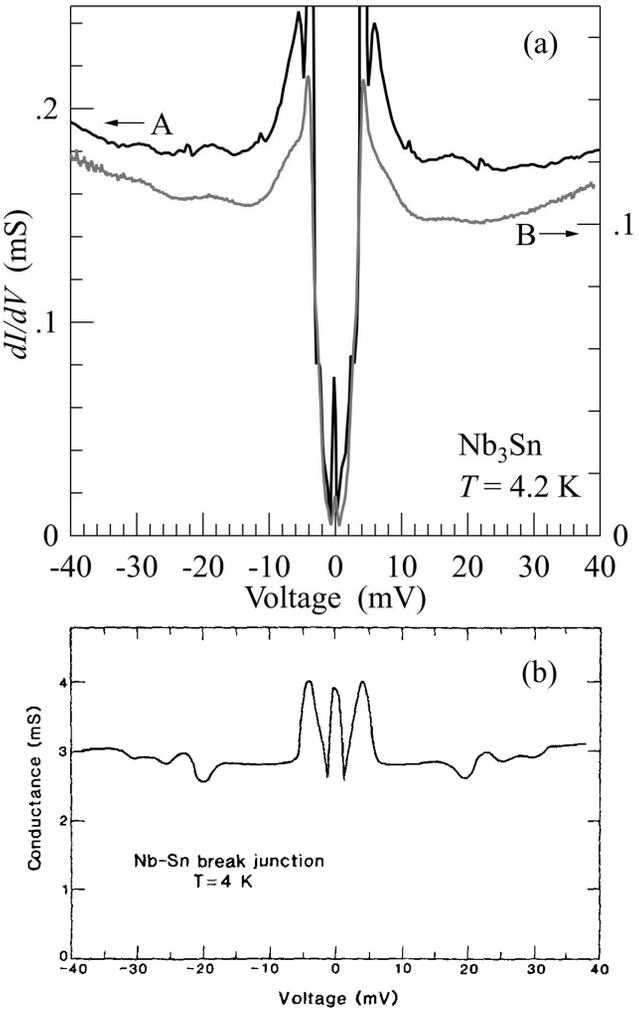

Figure 4. (a) $G(V)$ describing different Nb_3Sn break junctions. (b) The break-junction data of the superconducting Nb-Sn composite (taken from Ref. [30]).

proximity between different phases rather than features appropriate to a true two-gap superconductivity realized in the momentum-space [20].

In addition to the superconducting-gap structures at ≈ ±4.2–4.6 mV and ≈ ±5.5 mV, one can see the broad humps around ±20 mV as a third structure inherent to the curves A and B in Figure 4 (a). The hump bias positions and their ≈2–4% intensity increase against the background are similar for all curves represented. Such ±20 mV structures were also seen previously in Nb-Sn break junctions [30] and an example is shown for comparison in Figure 4 (b). In those data (Figure 6 of Ref. [30]), the peculiarities start at ±20 mV and extend up to biases of ±30 mV. Their subtle intensity could be associated with their possible origin as strong-coupling phonon features, phonons being the most probable Cooper-pair glue in Nb_3Sn. However, this explanation seems to be unlikely here because similar hump structures are observed together with the smaller ±4.3 mV superconducting-gap peaks, corresponding to the phase with a lower T_c, but in the absence of the larger ±5–6 mV ones, which are considered as the predominant gap features. Furthermore, although the strong-coupling feature of the electron–phonon interac-

tion should be concomitant with the ideal BCS-like gap structures, no such hump is observed along with the very distinct BCS gap structure of Figure 3 (a). On the other hand, it seems remarkable that the coexisting superconducting-gap and hump structures presented here are very similar to the tunnelling conductance patterns of the high-T_c copper-oxide superconductors observed at low T [16, 33], although the energy scales differ in both cases [27]. We note that a misleading interpretation of the outer structures as a strong-coupling effect was discussed earlier in the case of a 5*f*-electron superconductor [40].

We plot the temperature evolution of $G(V)$ in Figure 5 for a mechanically stable break-junction configuration. This is a representative selected among a number of trial measurements. The conductance $G(V)$ at each T, $G(V, T)$, is quite stable exhibiting almost no shift along the vertical $G(V)$ axis in the whole T range from 4.2 K to 20 K. It might be expected that thermal crystal lattice expansion would destroy the conventional smooth evolution with T of the $G(V)$ spectra, but in our case this possible disturbance is completely absent or cancels out. To be certain that this stability of spectra really takes place, we even sometimes measured $G(V)$ with the T-steps up to several tenths of Kelvin and no shift was noticed just the same. The microscopic origin of the observed mechanical stability still remains to be clarified, but it can be speculated that the exposed edges of the fractured crystal may accompany structural changes by possible surface reconstructions, which might serve as solid junction interfaces. In Figure 5, the well-defined gap-edge peaks clearly seen at $T = 6.4$ K are gradually suppressed and smeared when T increases and finally the sequence $G(V)$ tends to the curve of the shallow V-like shape at T about 17.4 K. This behaviour is quite common to the BCS superconductors.

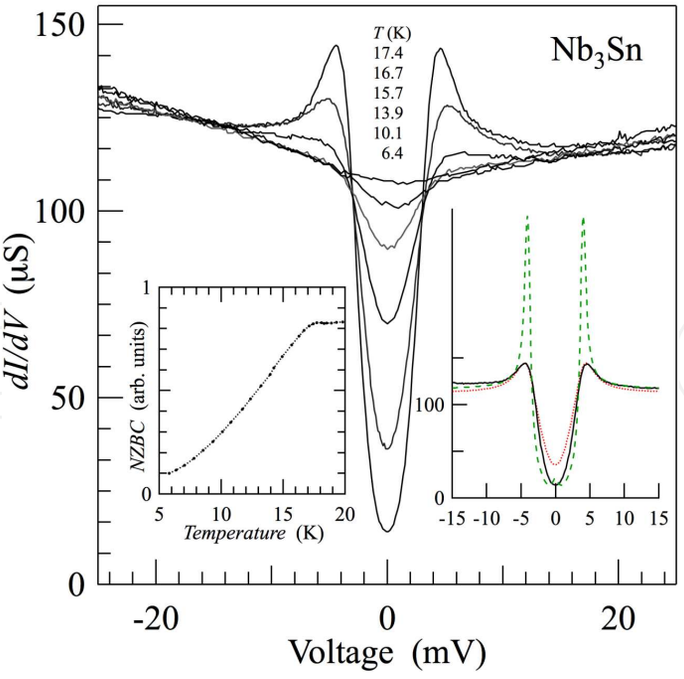

Figure 5. Temperature variations of $G(V)$ for an Nb_3Sn break junction. The left inset shows the temperature dependence of the normalized zero-bias conductance, $G(0)/G$ (±30 mV). The right inset shows the $G(V)$ fitting with $N(E, \Gamma)$ for the SIS junction (see the text).

To analyze the T-driven evolution of the gap characteristics more closely, we plot the T dependence of the fixed conductance at zero bias, $G(0, T)$, normalized by high-bias voltage value (V = 30 mV) in the left inset of Figure 5. It is noted that $G(0, T)$ changes drastically, while the conductance at 30 mV, G(30 mV, T), is kept almost constant. According to the BCS theory for isotropic superconductors, the quantity $G(0, T)$ is proportional to the thermally smeared convolution of two densities of states. Thus, $G(0, T)$ may serve as an estimate of the removed electronic states due to the superconducting-gap formation with decreasing T. For a typical SIS junction, however, the intensive Josephson peak and thermally excited states above and below the gap energy made it impossible to quantitatively measure the smooth $G(0, T)$. Nevertheless, in the left inset of Figure 5, the actual $G(0, T)$ can be of help to estimate the gap evolution because of the featureless zero-bias conductance similar to that for an SIN junction.

The critical temperature T_c of Nb_3Sn at the break-junction interface should be determined as ≈18 K from the behaviour of the zero-bias conductance $G(0, T)$, which is consistent with the temperature dependence of the electrical resistance, $R(T)$, in the Figure 2. The low-T gap combined with the found value $T_c \approx 18$ K gives the gap-to-T_c ratio $2\Delta(0)/k_BT_c \approx 2.8–2.9$, which is notably smaller than the weak-coupling BCS constant 3.5, not to talk about the strong-coupling values ~4.4 known from literature [10, 28]. After a closer look at the left inset of Figure 5, one can recognize that $G(0, T)$ has a very weak maximum below 18.3 K and exhibits a decrease with lowering T, the slope becoming steeper below 14–15 K. The latter threshold T value is consistent with the local BCS $T_c^* \approx 14–15$ K corresponding to $2\Delta = 4.2–4.6$ meV as was inferred from Figure 3 (a). This smaller gap is probably formed by the proximity effect in the junction region presumably due to the break-junction fracture of the local imperfect phase. The subtle rising of the peak in $G(0, T)$ with the decrease of T below ≈18.3 K, may correspond to the BCS coherence-factor manifestation below T_c due to the energy gap formation. The right inset shows the SIS conductance fitting results using the $N(E,\Gamma)$ with thermal smearing in order to determine accurately the gap value at 6.4 K [39]. We can recognize from these results that the fitted gap-peak position corresponding to the gap parameter Δ = 2–2.3 meV changes only slightly even if the broadening parameter Γ varies strongly in the range 0.12–0.46 meV.

Figure 6 displays the conductance curve $G(V)$ extended to the high-bias region. We can notice larger-V features in addition to the superconducting-gap-edge structures. The magnitude of $G(V)$ exhibits rather weak voltage dependence up to $|V| \approx 100$ mV. In the curve A of Figure 6, the width of the central superconducting-peak region is about 9 mV, which corresponds to the representative gap value 2Δ = 4.5 meV as has been already indicated and discussed in connection with Figures 3–5. The main and unconventional features of $G(V)$ shown in the curve A of Figure 6, which deserve to be emphasized, are the reproducible broadened humps of $G(V)$ centered at biases ≈ ±50–60 mV with the shallow depression between them. This hump structure in $G(V)$ possesses the overall change in $G(V)$ ~20% of the background. One finds the gap-like peaked structures beyond the central region that reveal superconducting-gap peculiarities and subtle features at -20 mV as discussed in the text concerning Figure 4.

The ±50–60 mV gap-like structures were also obtained for the different junction as is shown in curve B of Figure 6. The curve exhibits bends or kinks in this case, which exhibit a weaker change (≈5%) against the background $G(V)$ value, but their bias positions at ± ~50 mV are in

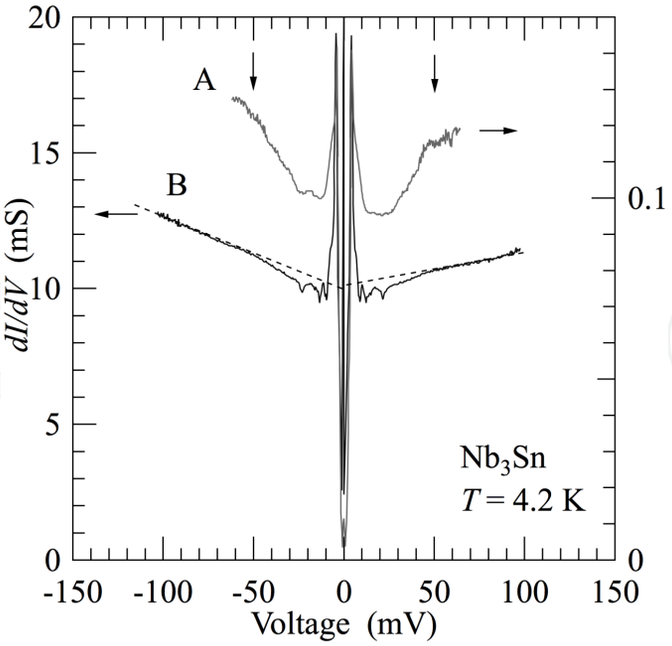

Figure 6. $G(V)$ for Nb_3Sn break junctions in the bias range up to ±150 mV.

accordance with each other. This fact testifies that the structures observed in this bias region have a common origin. Anyway, the subtle peak features at ±20 mV are well reproduced and most probably have the same origin as discussed in the context of Figure 4. In curve B, the ±5.5 mV superconducting-gap-edge peaks corresponding to the bulk $T_c \approx 18$ K are seen as well. All the features including the conventional superconducting gap of ±4.5 mV are reproduced in curve B regardless of the conductance $G(V)$ magnitude, which is ~10^2 times larger than that of curve A. From these patterns, the reproducible characteristic structures at ±5.5 mV, ±20 mV, ±50 mV inherent to Nb_3Sn are confirmed.

Further measurements above T_c were carried out in order to be sure that the above hump structures are not due to the superconductivity-induced spurious effects. Figure 7 shows the tunnelling spectra for different break junctions at temperatures 4.2 K (Figure 6, curve B) and above T_c. The mechanically supported break junctions go usually very unstable at high temperatures. Therefore, we could not ubiquitously obtain certain spectral features for all the junctions. Nevertheless, as shown in Figure 7, the tunnelling conductance spectra show reproducible gap-edge-like structures at characteristic biases around ±50 mV, which are in agreement with the hump structures appropriate to the conductance measured when the junction electrodes were at lower temperatures, deep in the superconducting state. The biases of the apparent gap-edge-like structures are distributed around the ±40–60 mV range. Similar scattered characteristic bias positions already appeared in the low-temperature superconducting data depicted in Figure 6. We should emphasize here that the very existence of the energy gap in the normal state above T_c is remarkable for Nb_3Sn.

Comparison of the substantially suppressed sub-gap conductance features for the normal-state data of Figure 7 with the extrapolated zero-bias conductance values of curve A in Figure 6 indicates that a sufficient quality of the junction interface should be realized to notice the partial

http://dx.doi.org/10.5772/59338

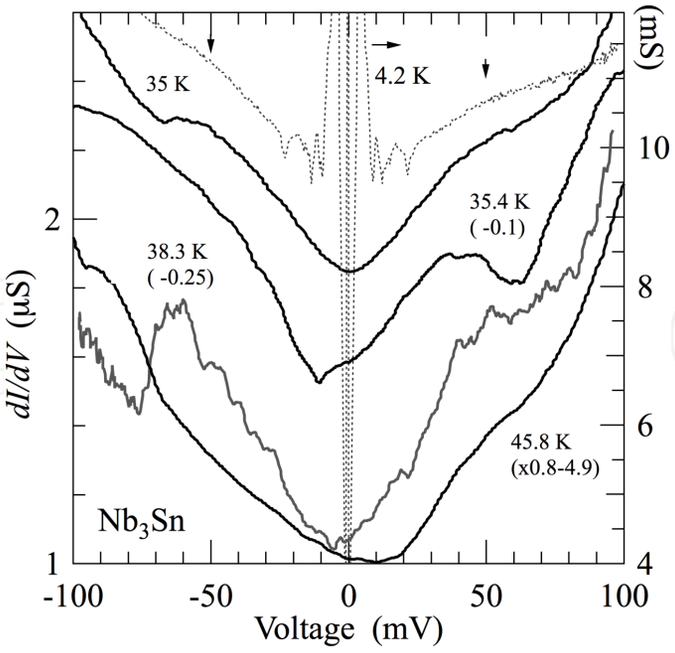

Figure 7. $G(V)$ for different Nb_3Sn break junctions well above T_c up to 45.8 K.

density-of-states gapping in the quasi-particle tunnelling studies. The zero-bias conductance depression values are noted to constitute about 30% of the normal state conductance. Therefore, assuming the SIS geometry of the break junction, one can estimate that about 17% of the density of states $N(E_F)$ at the Fermi energy E_F was removed due to formation of the normal-state gap with the position at about ±50–60 mV. The gap structures in $G(V)$ above 35 K depicted in Figure 7 exist well above the bulk $T_c \approx 18$ K. Each $G(V)$ curve corresponds to its own break junction. One observes reproducible gap-edge-peak positions ±40–60 mV in the conductance spectra. Such characteristic values are kept almost constant together with the inner gap structures. The asymmetric gap structures obtained for the symmetric break-junction configuration testify that the single-crystalline samples were cracked along defects or grain boundaries, resulting in the conspicuously asymmetric junction properties. Although the highest temperature of measurements was 45.8 K, it is remarkable that the gap locations at 50 mV are almost the same as the hump positions found at 4 K in the superconducting state.

Since the smaller features at ±20 mV of Figure 4 displayed in the superconducting state are approximately reproduced, the peculiarities found at this bias range and reported previously for Nb_3Sn [25–30], which have been attributed to the electron–phonon interaction manifestations in the spectra for this compound, should be rather considered as the gap-edge structures of a non-superconducting nature. Since the present observations seem to be important in order to interpret the Nb_3Sn tunnelling characteristics found previously, we collected various tunnel spectra in Figure 8. As shown, the ±20 mV structures manifest themselves regularly at temperatures from 4.2 K up to 35 K, well above T_c.

The significant conductance asymmetry with respect to the bias as is demonstrated in Figures 7 and 8 was observed in the majority of the tunnelling experiments dealing with the normal-

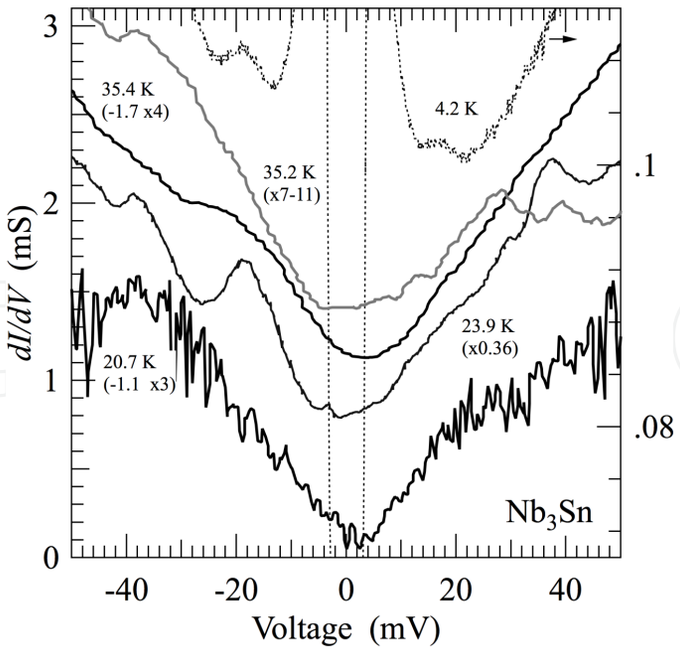

Figure 8. $G(V)$ for different Nb_3Sn break junctions showing mainly the smaller ±20–30 mV gap structures.

state gap or the dip-hump structures in high-T_c cuprate superconductors [33]. Such asymmetries can be naturally understood by considering the phase of the CDW order parameter. This phase may enter and substantially distort the quasi-particle tunnelling characteristics in the partially CDW-gapped and at the same time partially normal-metal state formed in the symmetric set-up of the break junction between CDW conductors if the symmetry is somehow violated. In particular, her hand, appearance of this asymmetry, together with the manifestations of double-gap features at both inner biases of ±20–30 mV and almost twice larger values ±50 mV, indicates that the gap structures possessing the smaller values ±20 mV are probably due to the asymmetric junction formation with the CDW gap Σ and the conductance featured at $V = \pm \Sigma/e$. The dissimilarity between $G(V)$ branches in apparently symmetric junctions may be a consequence of the broken symmetry phenomenon [15, 33]. In this case, both electrodes are in the same CDW-gapped state but with Σ_{left} and Σ_{right} having different signs! Alternatively, an asymmetric junction might be formed after cracking the sample with one of the electrodes being in a CDW-free metallic state. Then $G(V)$ is also asymmetric [15, 33].

Possible emergence of extra gapping due to the CDW influence on the Nb_3Sn tunnel spectra makes ambiguous the routine interpretation of extra $G(V)$ structures as the result of strong-coupling features induced by the electron–phonon interaction, although such an identification is familiar and often quite correct for more conventional superconductors [40]. Once such structures are recognized as the intrinsic gaps, like in our case, the difficulties of interpretation should be resolved taking into account the gapping by instabilities in the electron–hole channel. The weak hump structure depicted in Figure 4 is now understood as the $\pm \Sigma/e$ singularity emerging due to the partial Fermi surface CDW-driven gapping in the junction, its asymmetric form being induced by the broken symmetry in the CDW state with the opposite signs of CDW order parameters in the electrodes. On the other hand, as we have indicated

http://dx.doi.org/10.5772/59338

above, the asymmetric $G(V)$ shape of the apparently symmetric junction may emerge due to the actual formation of the asymmetric (one-side normal-metal) junction. In this case, the CDW-driven current-voltage characteristics are asymmetric for any phase of Σ except $\pi/2$ [15, 33]. The realization of the actually asymmetric configuration in the nominally symmetric junctions was observed in the break-junction measurements of both CDW conductors [41] and superconductors [42].

We attribute the normal-state gap features to the (martensitic) structural phase transition observed in the A-15 compound Nb_3Sn [1, 2, 13–15, 20, 24, 31, 34, 43], on the basis of the evidence given in the Introduction. Below the corresponding transition temperature, the cubic crystallographic symmetry is deformed and the tetragonal periodic lattice distortions appear driven by the Peierls-type instability due to the displacement of Nb atoms. The concomitant CDW leads to the quasi-particle gap formation in the parent electronic density of states $N(E)$. Since in Nb_3Sn the CDW transition hardly affects the transport properties [12], the dielectric energy gap Σ should distort only a small section of the Fermi surface. Its electronic signature is very weak and hence there were previously not so many discussions about the peculiarities of the tunnel conductance spectra characterizing Nb_3Sn junctions. Moreover, CDW distortions in Nb_3Sn seem to be spatially inhomogeneous similarly to what is inherent to cuprate layered structures [16, 33]. This would make the manifestations of the CDW peculiarity in the electron spectrum much smoother than in conventional cases of sharp second-kind phase transitions. Therefore, the CDW gapping reveals itself in the tunnelling $G(V)$ as a weak pseudo-gap-like feature well known for other objects [16, 17, 33, 44]. Actually, the average depth of the CDW-related gap-like structure constitutes less than half of the background. This is readily understood taking into account the inhomogeneity effects and the gapping of only a small Fermi surface section.

High-T measurements revealed the existence of the gap-like structure at 46 K, which is above the reported martensitic transition $T_m = T_{CDW} \approx 43$ K, and the gap-edge value does not decrease even at this temperature as compared with the low temperature data. This is in contrast to the apparent decrease of the normal-state gap energy above T_c reported by Escudero and Morales [31], although we agree with those authors that the gap feature survives above 45–50 K. Generally speaking, the inhomogeneity of the CDW structures should result in the scattered T_{CDW} values. The broad singularities at ±50–60 mV can be attributed to the CDW gap edges with $\pm 2\Sigma/e$ corresponding to the martensitic transition, which normally occurs at T_{CDW} [1, 2]. According to our data, T_{CDW} is in the range ≈46–50 K, so that the gap ratio $2\Sigma/k_B T_{CDW}$ can be estimated as ≈14±2. This value is significantly larger than the mean-field s-wave BCS ratio 3.53 describing the isotropic Cooper pairing. However, such values are typical for CDW phase transitions although their *reduced* gaps $\Sigma(T)/\Sigma(0)$ are well described by the BCS-like mean-field equations. For instance, $2\Sigma/k_B T_{CDW}$ is about 15 for the normal CDW transition in the low-dimensional conductor $NbSe_3$ [45].

Finally, it should be noted that the theoretical approach to the interplay between superconductivity and CDW phenomena, which started in connection to A-15 compounds [13], was recently successfully applied to treat the pseudo-gap manifestations in copper oxides [15–17,

33]. The presented observations strongly support the idea that certain phenomena in A-15 and high-*T* superconductors, in particular the dip-hump structures, are of the similar origin.

4. Summary

From the break-junction tunnelling measurements of the Nb_3Sn single crystals, the representative superconducting gaps were found to be $2\Delta = 4–4.5$ meV ($2\Delta/k_BT_c \approx 2.8$) and 5.5–6meV ($2\Delta/k_BT_c \approx 3.7$). The smaller gap is probably due to the proximity effect involving the Sn-deficient phase, while the larger one is naturally attributed to the bulk value. Hence, the two-gap superconductivity in Nb_3Sn confirmed here and found elsewhere is not an intrinsic two-gap superconductivity driven by two interacting distinct electron bands.

The high-bias tunnelling conductance exhibits gap-like structures with the characteristic values $2\Sigma = 50–60$ meV, which are observed up to at least ~50 K. These gaps can be due to the CDW pairing associated with the martensitic structural phase transition observed at $T_m \equiv T_{CDW}$. The gap ratio $2\Sigma/k_BT_{CDW}$ is estimated to be 14±2, which is typical for the known CDW conductors. Further measurements, with the emphasis on the higher temperature evolution of Σ, should be necessary to clarify the nature of the CDW-related phenomena in this A-15 compound.

Acknowledgements

This work was supported by a Grant-in-Aid for Scientific Research (24540377) of the Japan Society for the Promotion of Science (JSPS). The work was partially supported by the Project N 24 of the 2015–2017 Scientific Cooperation Agreement between Poland and Ukraine.

Author details

Toshikazu Ekino[1*], Alexander M. Gabovich[2], Akira Sugimoto[1], Yuta Sakai[1] and Jun Akimitsu[3]

*Address all correspondence to: ekino@hiroshima-u.ac.jp

1 Hiroshima University, Graduate school of Integrated Arts and Sciences, Higashihiroshima, Japan

2 Institute of Physics, National Academy of Science, Kiev, Ukraine

3 Aoyama-Gakuin University, Department of Physics, Sagamihara, Japan

References

[1] Testardi L RStructural instability and superconductivity in A-15 compounds :Rev. Mod. Phys.1975:47:(3637-648.

[2] Müller J;Al5-type superconductors Rep. Prog.Phys.1980:43:(5) 643-687.

[3] Cava R J: Oxide superconductors J. Am. Ceram. Soc.2000:83(1):5-28.

[4] Scanlan R M, Malozemoff A P, Larbalestier D C:Superconducting materials for large scale applications Proc. IEEE. 2004:92(10):1639- 1654.

[5] Gurevich A:To use or not to use cool superconductors? Nature Mater.2011:10(4): 255-259.

[6] Canfield P C:Still alluring and hard to predict at 100 Nature Mater. 2011:10(4): 259-261.

[7] Tarantini C, Gurevich A:High-field properties of pure and doped MgB2 and Fe-based superconductor MRS Bull. 2011:36(8):626-630.

[8] Kumakura H:Development and prospects for the future of superconducting wires Jpn. J. Appl. Phys. 2012:51(1):010003.

[9] Tanabe K,Hosono H: Frontiers of research on iron-based superconductors toward their application Jpn. J. Appl. Phys.2012:51(1):010005.

[10] Godeke A:A review of the properties of Nb3Sn and their variation with A15 composition,morphology and strain state Supercond. Sci. Technol. 2006:19(8):R68.

[11] Godeke A, tenHaken B,tenKate H H J,Larbalestier D C: A general scaling relation for the critical current density in Nb3SnSupercond. Sci. Technol. 2006:19(10):R100.

[12] Gorkov L PProperties of A15 compounds and one-dimensionality : In: Progress in Low Temperature Physics, Vol.VIIB.ed.Brewer D F: North Holland, Amsterdam: 1978.518-589 p.

[13] Bilbro G,McMillan W L:Theoretical model of superconductivity and the martensitic transformation in A15 compounds Phys. Rev. B1976:14(5):1887-1892.

[14] Nakayama J: {Structural transformations and superconductivity in A15 compounds J. Phys. Soc. Jpn.1977:43(5):1533- 1538.

[15] Gabovich A M, Voitenko A I,Ausloos M: Charge-density waves and spin-density waves in existing superconductors: competition between Cooper pairing and Peierls or excitonic instabilities Phys. Rep.2002:367(6):583- 709.

[16] Ekino T,Gabovich A M, LiMai Suan, Pękała M,Szymczak H, VoitenkoAI;Analysis of the pseudogap-related structure in tunneling spectra of superconducting Bi2Sr2Ca-Cu2O8+δ revealed by the break-junction technique Phys. Rev. B. 2007:76(18):180503.

[17] Ekino T, Gabovich A M, LiMai Suan,Pękała M,Szymczak H, Voitenko A I: The phase diagram for coexisting d-wave superconductivity and charge-density waves: cuprates and beyond J. Phys. Condens. Matter. 2011:23(38):385701.

[18] Ekino T,Gabovich A M, LiMai Suan, Takasaki T, Voitenko A I, Akimitsu J, Fujii H, Muranaka T, Pękała M P, Szymczak H:Spatially heterogeneous character of superconductivity in MgB2 as revealed by local probe and bulk measurements Phys. C. 2005:426-431:230-233.

[19] Ekino T, Sugimoto A, GabovichA M: Scanning-tunneling microscopy/spectroscopy and break-junction tunneling spectroscopy of FeSe1–xTex Fiz. Nizkikh Temp. 2013:39(3):343-353.

[20] Zehetmayer M: A review of two-band superconductivity: materials and effects on the thermodynamic and reversible mixed-state propertiesSupercond. Sci. Technol. 2013:16(4):043001.

[21] Vieland L J, Wicklund A W: Specific heat of niobium-tin Phys. Rev. 1968:166(2): 424-431.

[22] Guritanu V, Goldacker W, Bouquet F, Wang Y, Lortz R, Goll G, Junod A: Specific heat of Nb3Sn: The case for a second energy gap Phys.Rev. B. 2004:70(18):184526.

[23] Marz M, Goll G, Goldacker W, Lortz R: Second superconducting energy gap of Nb3Sn observed by breakjunction point-contact spectroscopy Phys.Rev. B. 2010:82(2):024507.

[24] Escudero R, Morales F, Bernès S: Specific heat studies of pure Nb3Sn single crystals at low temperature J. Phys. Condens. Matter.2009:21(32):325701.

[25] Shen L Y L: Tunneling into a high-*Tc* superconductor - Nb3Sn Phys. Rev. Lett. 1972:29(16):1082-1086.

[26] Vedeneev S I, GolovashkinA I, Levchenko I S, Motulevich G P: Investigation of tunnel characteristics of sputtered superconducting Nb3Sn films ZhurnÉksp. Teor. Fiz. 1972:63(3):1010-1019 [Sov. Phys. JETP. 1973:36(3):531-535].

[27] Wolf E L, Zasadzinski J, Arnold G B, More D F, Rowell J M, Beasley M R: Tunneling and the electron-phonon-coupled superconductivity of *Nb*3Sn Phys.Rev.B. 1980:22(3):1214-1217.

[28] Rudman D A, Hellman F, Hammond R H, Beasley M R: A15 NbSn tunnel junction fabrication and properties J. Appl. Phys. 1984:55(10):3544-3553.

[29] Geerk J, Kaufmann U, Bangert W, Rietschel H: Electron tunneling into *Nb*3Sn, *Nb*3Ge, and *Nb*3Al Phys. Rev. B. 1986:33(3):1621-1626.

[30] Moreland J, Ekin J W: Electron tunneling experiments using NbSn ''break'' junctions J. Appl. Phys. 1985:58(10):3888-3895.

[31] Escudero R, Morales F: Point contact spectroscopy of Nb3Sn crystals: Evidence of a CDW gap related to the martensitic transitionSolid State Commun. 2010:150(15-16): 715-719.

[32] Kopaev Yu V: About the interplay theory between electron and structural transformations and superconductivity Trudy FIAN.1975:86:3-100.

[33] Gabovich A M, Voitenko A I, Ekino T,Li M S,Szymczak H, Pekala M: Competition of superconductivity and charge density waves in cuprates: Recent evidence and interpretation Adv. Condens. Matter Phys. 2010:2010:681070.

[34] Bhatt R N: Microscopic theory of the martensitic transition in *A*−15 compounds based on a three-dimensional band structure Phys. Rev. B. 1977:16(5):1915-1932.

[35] Tütüncü H M, Srivastava G P, Bağci S, Duman S: Theoretical examination of whether phonon dispersion in Nb3Sn is anomalous Phys. Rev. B. 2006:74(21):212506.

[36] Barone A, Paterno G: The Physics and Applications of the Josephson Effect: Johney and Sons, New York: 1982, 529pp.

[37] Coleman R V, Giambattista B, Hansma P K, Johnson A, Mcnairy W W,Slough C G: Scanning tunnelling microscopy of charge-density waves in transition metal chalcogenides Adv. Phys. 1988:37(6):559-644.

[38] Ekino T, Takabatake T, Tanaka H, Fujii H: Tunneling evidence for the quasiparticle gap in Kondo semiconductors CeNiSn and CeRhSb Phys. Rev. Lett. 1995:75(23): 4262-4265.

[39] Dynes R C, Narayanamurti V, Garno J P: Direct measurement of quasiparticle-lifetime broadening in a strong-coupled superconductor Phys. Rev. Lett. 1978:41(21): 1509-1512.

[40] Geerk J, Lohneysen H v: Convolution effects in superconductive tunneling Phys. Rev. Lett. 2007:99(25):257005.

[41] Jung M H, Ekino T, Kwon Y S, Takabatake T: Tunneling spectroscopy of RTe2 (R = La, Ce) and possible coexistence between charge-density waves and magnetic order-Phys. Rev. B. 2001:63(3):035101.

[42] Ekino T, Fujii H, Kosugi M, Zenitani Y, Akimitsu J: Tunneling spectroscopy of the superconducting energy gap in *R*Ni2B2C (*R* = Y and Lu) Phys. Rev. B. 1996:53(9): 5640-5649.

[43] Ekino T, Sugimoto A, Sakai Y, GabovichA M, Akimitsu J:Fiz. Tunneling spectra of break junctions involving Nb3Sn Nizkikh Temp. (2014):40(10):1182-1186.

[44] Monceau P: Electronic crystals: an experimental overview Adv. Phys. 2012:61(4): 325-581.

[45] Ekino T, Akimitsu J: Electron tunneling study of NbSe3 Jpn. J. Appl. Phys. Suppl. 1987:26(Supplement 26-3):625-626.

IntechOpen